A vortex-based model of velocity and shear stress in a partially vegetated shallow channel

Brian L. White[1] and Heidi M. Nepf[2]

Received 11 June 2007; accepted 22 August 2007; published 8 January 2008.

[1] This paper presents a method for predicting the distributions of velocity and shear stress in shallow channels with a boundary of emergent vegetation. Experiments in a laboratory channel with model vegetation show that the velocity profile exhibits a distinct two-layer structure, consisting of a rapidly varying shear layer across the vegetation interface and a more gradual boundary layer in the main channel. In addition, coherent vortices are observed which span both layers, and are the dominant contributors to lateral momentum fluxes. From these observations, we propose a model for the vortex-induced exchange and find expressions for the width of momentum penetration into the vegetation, the velocity and shear stress at the vegetation edge, and the width of the boundary layer in the main channel. These variables, along with a momentum balance in the main channel, comprise a modeling framework which accurately reproduces the observed velocity and shear stress distributions. The predictions for the velocity and shear stress can provide a basis for modeling flood conveyance, overbank sediment transport, and scalar residence time in the vegetated layer.

Citation: White, B. L., and H. M. Nepf (2008), A vortex-based model of velocity and shear stress in a partially vegetated shallow channel, *Water Resour. Res.*, *44*, W01412, doi:10.1029/2006WR005651.

1. Introduction: Flows on Vegetated Floodplains

[2] Channels with fringing vegetation are found in many important environmental settings. Lowland rivers and their associated floodplains, coastal salt marshes with bank vegetation, and estuarine channels with fringing mangroves are a few examples. The exchange of mass and momentum between the high-discharge main channel and the more quiescent vegetated floodplain is of fundamental importance. This exchange establishes the shear stress at the bank, influencing the total discharge of the coupled system as well as erosion and bank stability. The exchange also influences the overbank transport of suspended sediment, with implications for the sediment budget of the marsh or floodplain, and it controls the flushing of biological or chemical constituents like larvae or nutrients, from the vegetated region, with obvious ecological implications.

[3] We consider a channel-vegetated-bank system consisting of an open channel partially filled with an array of cylindrical surface-piercing plants. This morphology is representative of emergent vegetation like reeds and rushes. We are interested in cases where the flow is sufficiently shallow to be approximately two-dimensional. A front and plan-view are shown in Figure 1. The vegetation properties are the characteristic diameter, d, the solid volume fraction, $\phi = (\pi/4)d^2n$, where n is the number of cylinders per unit bottom area (and $\phi = 1 - porosity$), the mean spacing between cylinders, $s = \sqrt{d/a}$, and the mean projected area per unit volume $a = nd$. The streamwise, lateral, and vertical coordinates and velocities are (x, u), (y, v), and (z, w), respectively. A typical streamwise velocity distribution is characterized by U_1, the mean velocity within the vegetation, spatially averaged to remove plant-scale fluctuations, and U_2, the (constant) velocity in the main channel and the velocity difference, $\Delta U = U_2 - U_1$. The velocity in each zone results from the balance between the pressure gradient (or the potential gradient due to bed slope) and the hydraulic resistance, imposed by the stems within the vegetation, and the bed friction in the channel. The slip velocity, U_s, is the difference between the mean velocity within the vegetation and the velocity at the interface.

[4] Several workers have studied the flow in composite channels with a vegetated floodplain, primarily in laboratory settings. Most models have used simplified one-dimensional approaches with an empirical Darcy-Weisbach friction factor or a simple eddy viscosity model for the turbulence structure. *Vionnet et al.* [2004] proposed an eddy viscosity model to describe the momentum exchange between the main channel and the floodplain, and used results from a laboratory model to calibrate it. *Helmiö* [2004] also used a one-dimensional model, with a calibrated Darcy-Weisbach friction factor at the vegetation interface, to describe the flow conveyance of two lowland rivers. However, these one-dimensional models do not describe the lateral distribution of velocity, or the turbulence structure.

[5] *Ikeda et al.* [1991] developed a more detailed two-dimensional approach with an eddy viscosity model to predict the lateral distribution of velocity and used it to model the sediment transport into the vegetation. The eddy

[1]Department of Physical Oceanography, Woods Hole Oceanographic Institution, Woods Hole, Massachusetts, USA.
[2]Department of Civil and Environmental Engineering, Massachusetts Institute of Technology, Cambridge, Massachusetts, USA.

0043-1397/08/2006WR005651$09.00

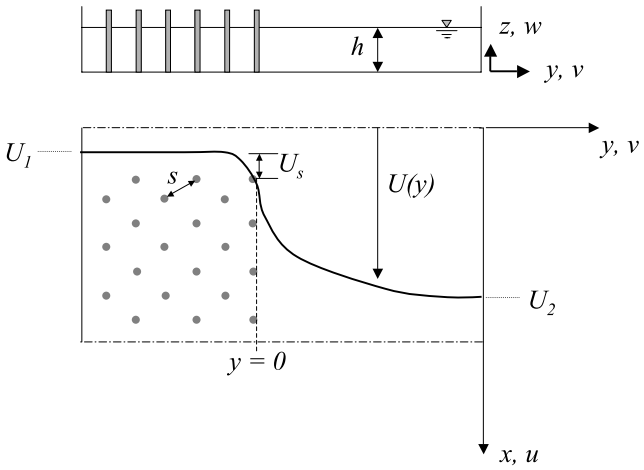

Figure 1. Problem description. Shallow laboratory channel with an array of emergent circular cylinders. The time-averaged streamwise velocity is $U(y)$ (down the page), the cylinder spacing is s, the slip velocity is U_s, and the overall velocity difference is $\Delta U = U_2 - U_1$. The streamwise, lateral, and vertical coordinates are x, y, and z, respectively.

viscosity was obtained by empirical fit to data. *Pasche and Rouvé* [1985] employed a two-dimensional model which divides the channel into three zones: the main channel, the vegetated plain, and a communication zone between them. They noted that the interfacial shear stress, acting on the plane between the channel and the vegetation edge is the essential link to describe the system. However, their analysis relies on a number of empirical relationships which provide neither a clear picture of the physics nor a framework for extending the results to general floodplains.

[6] Though the above two studies model lateral variability and communication between the main channel and floodplain, they do not consider the shear layer vortices that are known to form at the interface. These have been recognized in laboratory studies by *Tamai et al.* [1986] and *Nezu and Onitsuka* [2000]. The measurements of *Tamai et al.* demonstrated the coherent vortices were driven by a Kelvin-Helmholtz instability similar to that found in a free shear layer. *Nezu and Onitsuka* measured the turbulence structure and observed vortices initiated by the unstable inflection point at the vegetation interface. Large Eddy Simulation (LES) models by *Nadaoka and Yagi* [1998] and *Xiaohui and Li* [2002] have also been successful at capturing these vortices.

[7] A model was proposed by *van Prooijen et al.* [2005] for the momentum exchange between a channel and a shallow floodplain that includes the physics of the vortices and thus appears to be the most insightful model to date. However, their use of an eddy viscosity model with a constant mixing length across the floodplain interface does not capture the very sharp decrease in the turbulent length scale on the floodplain due to the high resistance, and as a result, the penetration of momentum onto the floodplain is slightly overpredicted. This problem will be even more severe for a vegetated floodplain, because of its even greater resistance. In this paper, we demonstrate that the region of shear is in fact comprised of two regions, a region of very sharp transition containing an inflection point, and a region of more gradual transition in the main channel in which the velocity resembles a boundary layer. Each region has its own distinct length scale and should be treated separately.

[8] We begin by describing the two-layer structure observed in the mean lateral velocity profiles in a shallow channel with model vegetation. Based on the data we describe relationships for the momentum penetration width into the vegetation and the velocity at the interface. We then describe observations of coherent vortices at the vegetation interface and develop a model for the lateral shear stress. Finally a model is presented which can be used to predict the velocity and shear stress distributions throughout the partially vegetated channel given only the vegetation characteristics, the bed friction, and the potential slope.

2. Experimental Setup

[9] Experiments were carried out in a 1.2 m wide, 13 m long laboratory flume partially filled with a 40 cm wide array of 6.5 mm diameter wooden circular cylinders (see Figure 2), a model for emergent vegetation. The cylinders filled the full water depth, piercing the surface. At the leading edge the vegetated and open regions were separated by a 1.2-m-long splitter plate, which allowed the flow to develop separately within each region, and minimized cross-stream currents associated with the flow first encountering the array. The volume fraction of the model plants was varied across experiments between $\phi = 0.02$ and $\phi = 0.10$. Experimental configurations and results are summarized in Table 1. Simultaneous two-component velocity measurements were made in the horizontal plane with a Laser Doppler Velocimetry (LDV) system [see *White and Nepf*, 2007]. Lateral transects were made at mid-depth, and at various longitudinal positions downstream of the splitter plate. The mid-depth measurements were within 5% of the depth-averaged velocity, confirmed by several vertical velocity profiles, which showed the velocity to be nearly uniform over depth within the vegetation, and to have a standard logarithmic profile in the open channel. Finally, by synchronizing the velocity records we were able to educe the spatial streamline structure of the coherent vortices that appear in the shear layer. Details for this method are given in *White and Nepf* [2007].

[10] The depth, h, was varied between 5.5 cm and 15 cm, and each depth satisfied shallow flow conditions, with depth to width ratios less than 0.1. The channel and the cylinder array were wide enough to ensure the shear layer for all cases was unaffected by the flume side walls. A recirculating pump provided flows between 2–50 Ls^{-1} and Reynolds numbers of $O(10^3–10^4)$ based on flow depth, $Re_h = \rho U_2 h/\mu$, or momentum thickness, $Re_\theta = \rho(U_2 - U_1)\theta/\mu$.

[11] The free surface elevation at the upstream and downstream ends of the test section was measured with analog capacitance-based displacement gauges connected to an A/D board and sampled at 25 Hz. From the free surface gradient, dh/dx, the drag coefficient, C_D for the vegetation was then estimated from a balance between total array drag and the pressure gradient due to the free surface slope,

$$\frac{1}{2} C_D a U_1^2 = -g dh/dx \tag{1}$$

where U_1 is the cross-sectionally averaged velocity within the vegetation array. The free surface variation, dh/dx,

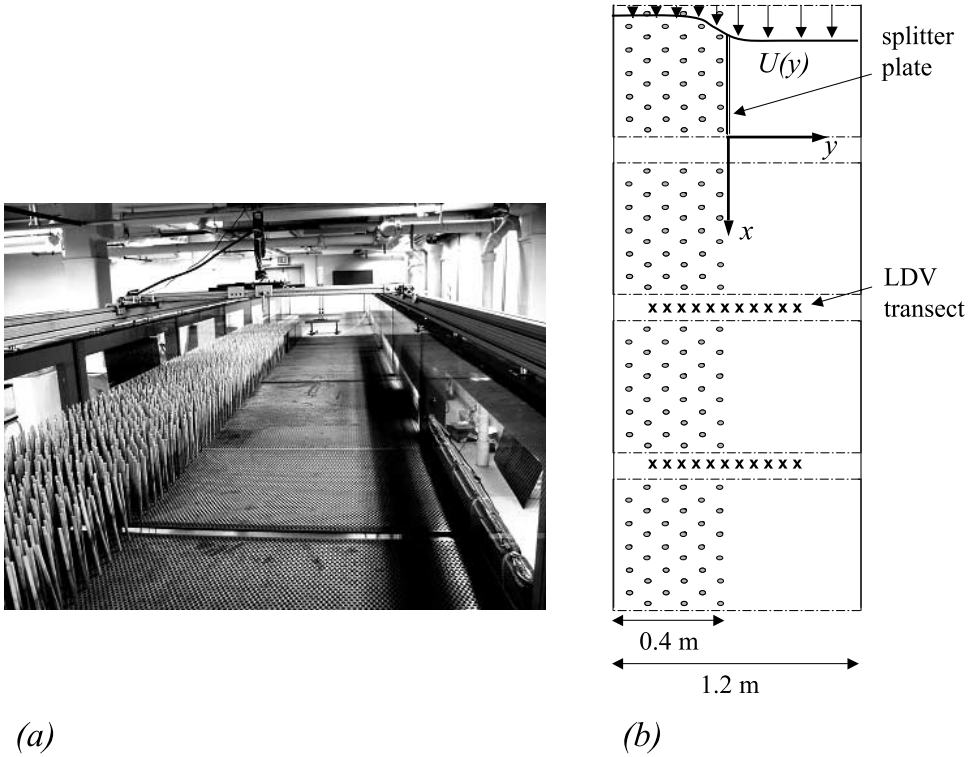

Figure 2. The laboratory setup. Photograph of the flume channel with model vegetation (a) and illustration of the model array with splitter plate and representative longitudinal spacing of the LDV transects (b). The streamwise, lateral, and vertical coordinates and velocities are (x, u), (y, v), and (z, w), respectively.

although dynamically important through the hydrostatic pressure forcing, has a negligible effect on the streamwise gradient of the streamwise velocity. The maximum slope was $0(1 \times 10^{-4})$, corresponding to relative variations in the water depth and the cross-sectionally averaged streamwise velocity of at most 1/100 over the length of the experimental section.

3. Experimental Results

3.1. Downstream Development

[12] The evolution of the lateral velocity profile with downstream distance from the splitter plate is shown in Figure 3a, for case IV. The mean velocity, $\langle \bar{U} \rangle$, has been time-averaged to remove turbulent fluctuations (overbar) and spatially averaged over the vegetation spacing, s, to remove plant-scale heterogeneity (angle brackets). As the flow adjusts, a transverse velocity component (not shown) carries fluid out of the vegetation, resulting in decreasing velocity within the vegetation and increasing velocity in the free stream. The shear layer width (Figure 3b), measured by the momentum thickness,

$$\theta = \int_{-\infty}^{\infty} \left[\frac{1}{4} - \left(\frac{\langle \overline{U} \rangle - (U_2 + U_1)/2}{\Delta U} \right)^2 \right] dy, \qquad (2)$$

Table 1. Experimental Parameters and Results for Each Case (From Equilibrium Profiles)

	I	II	III	IV	V	VI	VII	VIII	IX	X	XI
ϕ	0.020	0.020	0.020	0.045	0.045	0.045	0.10	0.10	0.10	0.10	0.10
$C_D a$ cm^{-1}	0.092	0.092	0.092	0.285	0.242	0.255	2.43	2.74	2.04	1.77	2.43
s (cm)	4.4	4.4	4.4	2.9	2.9	2.9	2.0	2.0	2.0	2.0	2.0
h (cm)	6.8	10.4	13.8	6.6	5.3	6.0	6.6	5.5	6.8	7.8	13.9
Re_θ	8.2×10^3	1.2×10^4	1.4×10^4	7.6×10^3	1.6×10^3	6.0×10^3	6.9×10^3	2.4×10^3	3.6×10^3	1.2×10^4	1.1×10^4
Re_h	2.0×10^4	3.0×10^4	1.0×10^4	1.8×10^3	6.7×10^3	1.0×10^4	2.9×10^3	5.6×10^3	2.1×10^4	2.8×10^4	1.1×10^4
U_1 (cms^{-1})	2.21	1.74	1.89	1.25	0.25	0.84	0.43	0.15	0.25	0.89	0.41
U_2 (cms^{-1})	17.68	21.69	23.97	17.37	3.82	12.32	16.82	5.85	9.05	29.59	22.02
u_* (cms^{-1})	1.81	2.27	2.67	2.06	0.35	1.48	1.93	0.44	0.84	3.44	2.51
U_s (cms^{-1})	3.68	5.12	5.59	3.72	0.80	2.52	3.41	1.03	1.79	6.11	4.51
y_o	1.34	1.91	1.41	−0.65	−0.24	−0.71	0.48	0.81	0.51	0.35	0.81
δ_I (cm)	3.71	6.03	6.20	2.61	2.19	1.89	1.24	0.89	1.06	1.34	1.35
δ_O (cm)	15.95	19.07	19.86	16.69	16.90	18.20	16.50	15.53	15.20	17.84	21.54
U_m (cms^{-1})	7.41	10.20	12.02	7.87	1.62	5.57	6.71	2.11	3.64	12.03	9.00
y_m (cm)	4.12	5.12	4.64	1.54	1.71	1.15	2.21	2.09	2.01	2.24	2.84
θ_{eq} (cm)	5.07	6.30	6.22	4.79	4.52	5.39	4.50	4.43	4.39	4.40	5.49

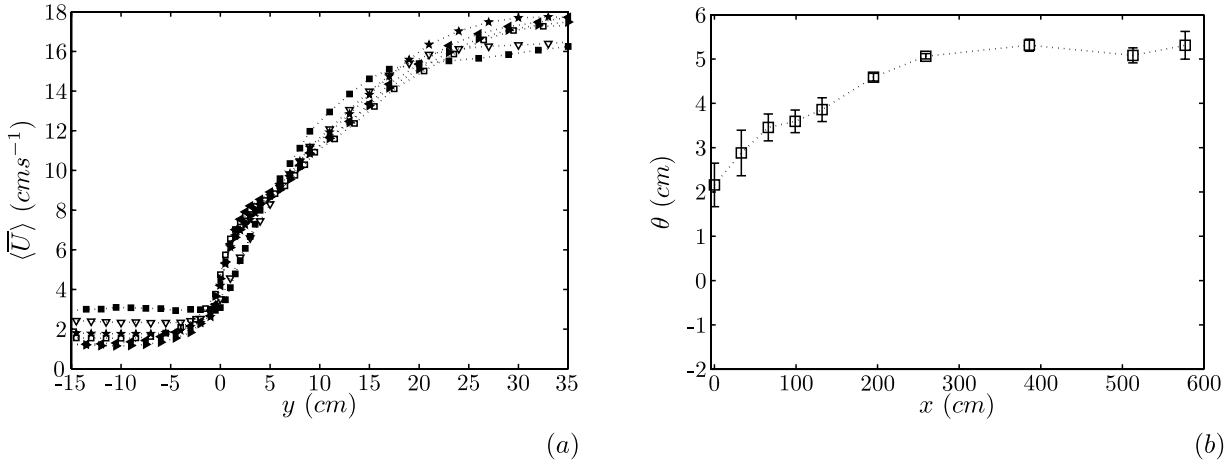

Figure 3. LDV measurements of shear layer growth (case IV). In Figure 3a, streamwise velocity at x = 33 cm (solid squares), x = 99 cm (open downward pointing triangles), x = 195 cm (stars), x = 386 cm (open squares), x = 513 cm (right pointing triangles), x = 577 cm (left pointing triangles). Only the region of shear is shown (-15 cm $< y <$ 35 cm), whereas actual flume dimensions are -40 cm $< y <$ 80 cm. In Figure 3b, the growth of the momentum thickness.

initially grows but asymptotes to approximately θ = 5 cm by $x \approx$ 400 cm, after which an equilibrium velocity profile is obtained (see the x = 386 cm profile in 3a).

3.2. Equilibrium Velocity and Reynolds Stress

[13] Equilibrium mean velocity profiles for various vegetation packing densities and Reynolds number are shown in Figure 4a. The data are laterally averaged within the vegetation zone, using a moving average filter of window length s, the cylinder spacing, in order to remove spatial heterogeneity created by the individual stems. The penetration of high momentum fluid and the velocity within the vegetation each decrease with density, but in the outer region, the velocity is nearly independent of density. In a separate paper [*White and Nepf*, 2007], we have shown that two distinct regions in the shear layer can be identified: (1) the region of high shear across the interface, which determines the length scale over which momentum can penetrate the vegetation, and (2) the region of shear outside the array, which determines the main channel boundary layer width. The region at the interface contains a velocity inflection point, similar to the mixing layer structure of vertical canopy flows [*Raupach et al.*, 1996]. However, the shear is asymmetric, as the velocity drops off rapidly into the vegetation, but is more gradual in the channel moving away from the vegetation. In the outer region the velocity profile resembles a boundary layer, with the vegetation interface playing the role of a (porous) wall. We refer to the two regions as the inner layer, with thickness δ_I, and the outer layer, with thickness δ_O, as shown in Figure 6.

[14] The equilibrium Reynolds stress profiles are shown in Figure 4b. There is a distinct peak that always coincides, to within measurement error, with the inflection point in the velocity profile. From the Reynolds stress maximum the shear stress at the interface, τ_i, and friction velocity, u_* can be defined,

$$u_*^2 = -\tau_i/\rho = \max\left(-\langle \overline{u'v'} \rangle\right). \tag{3}$$

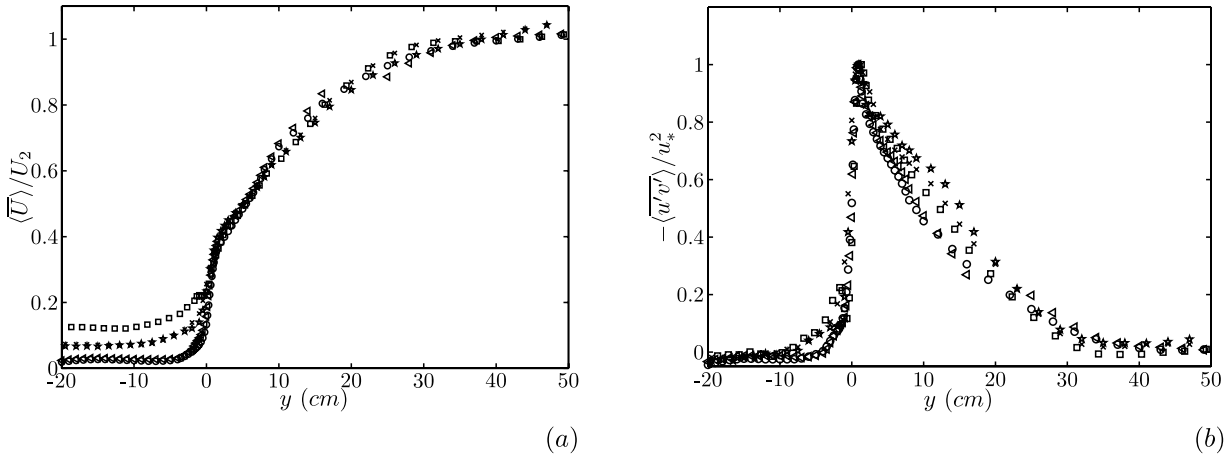

Figure 4. Equilibrium profiles of mean streamwise velocity (a) and Reynolds stress (b) across experimental conditions: case I (open squares), case IV (crosses), case VI (stars), case VII (open circles) and case X (left pointing triangles). Profiles are spatially averaged to remove cylinder-scale heterogeneity.

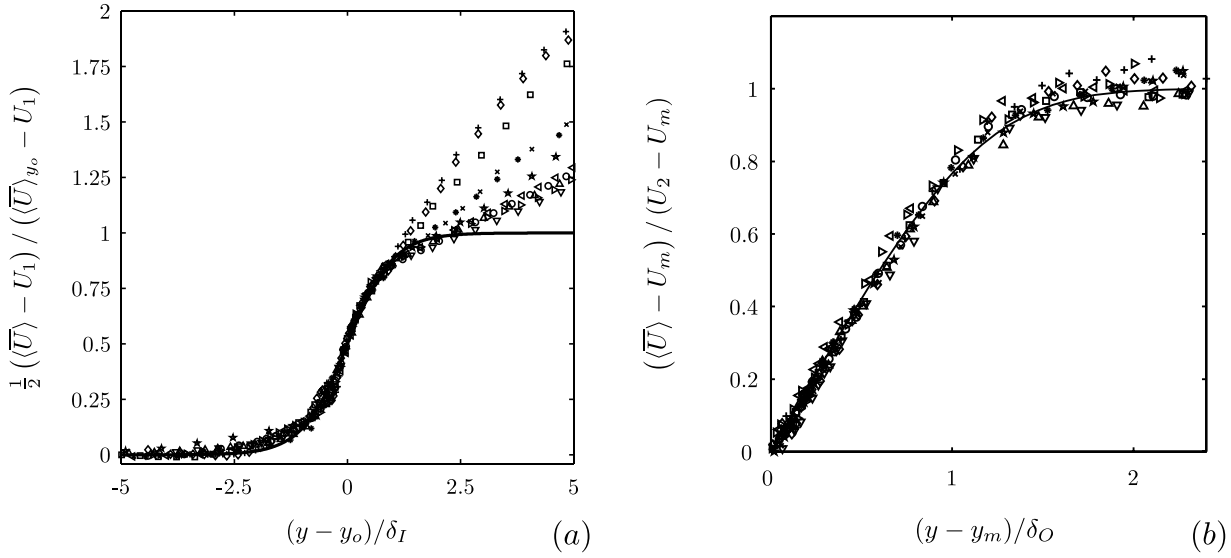

Figure 5. Two-layer scaling of the mean velocity. In Figure 5a, normalized inner layer profiles over all experimental conditions (spatially averaged) with hyperbolic tangent profile (solid line). In Figure 5b, rescaled outer layer profiles with parabolic boundary layer profile (solid line). The data, (from Table 1), are: open squares (I), open diamonds (II), pluses (III), crosses (IV), asterisks (V), stars (VI), open circles (VII), open upward pointing triangles (VIII), open downward pointing triangles (IX), open left pointing triangles (X), open right pointing triangles (XI).

[15] Thus u_* will define the magnitude of the shear stress at the boundary between the main channel and the vegetated plain.

[16] The velocity profiles for all cases collapse when nondimensionalized separately by the inner and outer layer scales (Figure 5). In Figure 5a, the inner layer profiles are shown after nondimensionalization by δ_I and offset by the inflection point location, y_o, which for all cases is within 1–2 cylinder diameters of the vegetation boundary. The profiles collapse to an S-curve, very close to the mixing layer structure of other canopy flows [*Raupach et al.*, 1996; *Ghisalberti and Nepf*, 2002; *Katul et al.*, 2002], which are well-described by a hyperbolic tangent profile (solid curve in Figure 5a). Alternatively, exponential or linear functions have been used to describe the velocity distribution near rough boundary layers [*Nikora et al.*, 2002], but these forms do not capture the inflectional point observed here. The hyperbolic tangent model of *Katul et al.* [2002] captures the inflection point but assumes that the mixing layer velocity profile is symmetric around the top of the roughness layer and is characterized by a single length scale. Our normalized velocity profiles follow the hypberbolic tangent curve very closely in the inner layer (Figure 5a), but diverge from the mixing layer form at a length of approximately $1.5\delta_I$ outside the vegetation boundary. In the outer layer, a separate boundary layer scaling holds (Figure 5b), and the velocity profiles collapse when normalized by δ_O, and offset by an origin and velocity, y_m and $U_m = U(y_m)$, the point at which the inner and outer layer slopes match (see section 4.3). The solid curve shown in 5b is a parabolic velocity profile (see (21) in section 5). This shape is consistent with a boundary layer established under the constraint of a constant eddy viscosity, analogous to Poiseuille flow. The good agreement with this parabolic profile guides our later analysis, as it will be demonstrated that a constant eddy viscosity is indeed appropriate in the outer region, leading to an explicit model for the velocity profile. Finally, a representative velocity profile illustrating both the inner and outer regions, along with important variables, is shown in Figure 6.

3.3. Coherent Vortices

[17] The most striking feature of the shear layer is the formation of regular coherent vortices, which make the greatest contribution to the turbulent shear stress. The vortices give the velocity time series a strong periodic signature. This is evident in Figure 7, which shows the fluctuating streamwise and transverse velocity components, along with their correlation, $u'v'$, the instantaneous Reynolds

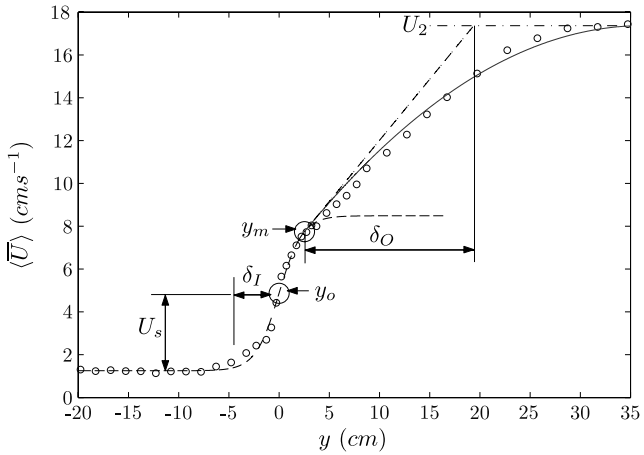

Figure 6. Representative profile demonstrating the inner layer (δ_I), outer layer (δ_O) velocity regions. The inner layer profile is the dotted line and the quadratic approximation to the outer layer is the solid line.

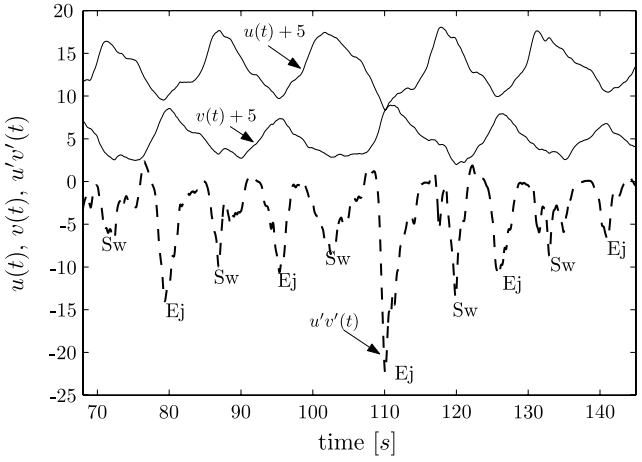

Figure 7. Time series of streamwise velocity, u, transverse velocity, v, (shifted for clarity) and instantaneous Reynolds stress, $u'v'$, measured near the interface, illustrating the periodic fluctuations with sweeps and ejections (labeled "Sw" and "Ej"). The frequency of the sweep/ejection cycle corresponds to the vortex frequency, f_n.

stress. The vortices create strong inflows, termed *sweeps* ($u' > 0$, $v' < 0$), and outflows, termed ejections ($u' < 0$, $v' > 0$), across the vegetation interface, which together make the dominant contribution to the average Reynolds stress, $\langle \overline{u'v'} \rangle$. The observed period of the vortices was consistently equal to

$$f_n = 0.032\overline{U}/\theta \tag{4}$$

where θ is the momentum thickness (2) and $\overline{U} = (U_1 + U_2)/2$ is the arithmetic mean velocity [for full results, see *White and Nepf*, 2007]. This is identical to the natural frequency predicted by linear stability theory for mixing layers [*Ho and Huerre*, 1984] and to the dominant frequency at which coherent structures have been observed in a submerged canopy flow [*Ghisalberti and Nepf*, 2002]. The frequency of the turbulent structures in the present shallow vegetated flow is therefore consistent with observations from vertical canopies.

[18] The vortex structure is revealed through the streamlines shown in Figure 8. The width of the vortices scales with δ_O, the outer layer width, for all flow and vegetation conditions. An ejection event, visualized by 10 μm reflective surface particles (trade name Sphericel), is shown in Figure 9. The image illustrates the significant length-scale over which transport occurs within an ejection event and the important role of the coherent structures in mass and momentum transport.

4. Framework for Predicting the Mean Velocity

[19] It is desirable to have a conceptual framework that can predict the velocity distribution and reproduce the observed two-layer structure. To do this, we will divide the flow into four separate zones: (I) the uniform region deep within the vegetated layer, (II) the inner layer at the interface (III) the outer boundary layer in the main channel and (IV) the region of uniform flow in the main channel outside the shear layer. These zones are shown in the vortex plot in Figure 8. In order to connect these regions, it will be necessary to know the width of the inner layer, δ_I, the interfacial slip velocity, U_s, and the interfacial shear stress, u_*^2. These three components are determined from both theory and experimental data in the following sections.

[20] To begin, the flow is governed by the balance of streamwise momentum. It is assumed that the mean velocity is steady and fully developed, i.e., $\partial/\partial x = 0$ and $\partial/\partial t = 0$. In addition, the Navier Stokes equations are Reynolds averaged in time, denoted by an overbar, and spatially averaged over depth and also horizontally over the vegetation spacing scale within the vegetation. The spatial averaging is denoted by angle brackets. The result is the following momentum balance,

$$-gS = \frac{1}{\rho}\frac{\partial \langle \tau_{xy} \rangle}{\partial y} - \langle \overline{D_x} \rangle \tag{5a}$$

where

$$S = -\frac{\partial h}{\partial x} \tag{5b}$$

is the free surface slope and

$$\langle \tau_{xy} \rangle = -\rho \langle \overline{u'v'} \rangle - \rho \langle (\overline{U} - \langle \overline{U} \rangle)(\overline{V} - \langle \overline{V} \rangle) \rangle \tag{5c}$$

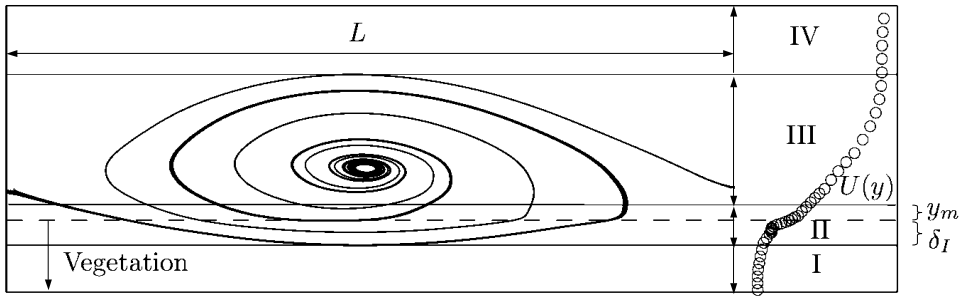

Figure 8. Streamlines for a typical vortex structure in a frame moving with the vortex. The vortices extend approximately $2\delta_O$ into the main channel and penetrate δ_I into the vegetation. There are four zones: the vegetated layer (I), the inner layer, which penetrates δ_I into the vegetation and extends y_m outside the vegetation (II), the outer layer in the main channel (III), and the region of uniform flow in the main channel (IV).

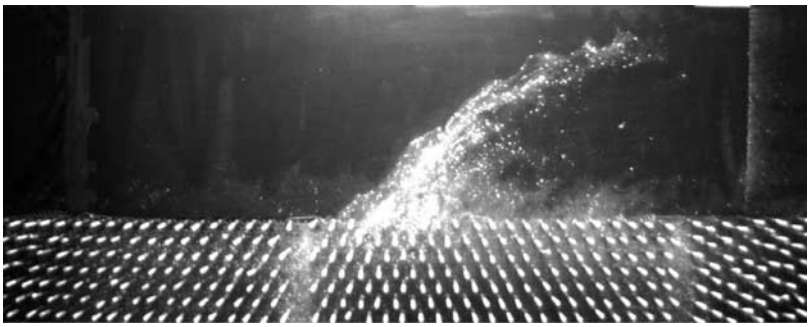

Figure 9. Visualization of a vortex ejection event, a strong outflow from the vegetation (flow is from left to right).

is the transverse shear stress, consisting of both a depth-averaged Reynolds stress (first term) and secondary circulations (second term). The stress due to secondary circulation was found to be at least an order of magnitude less than the Reynolds stress in the present experiments as well as in the study of *van Prooijen et al.* [2005] and is thus neglected from here forward. The total drag is a discontinuous function given by the sum of vegetation drag ($y < 0$) and the bed friction,

$$\langle \overline{D_x} \rangle = \begin{cases} \frac{1}{2}\left(C_D a + c_f/h\right)\langle \overline{U} \rangle^2, & y < 0 \\ \frac{1}{2}\left(c_f/h\right)\langle \overline{U} \rangle^2, & y > 0. \end{cases}, \tag{5d}$$

where C_D is the vegetation drag coefficient and c_f is the bed friction coefficient. For all situations of interest, $c_f/h \ll C_D a$, so bed drag is negligible within the vegetation.

4.1. Velocity Outside the Shear Layer: Zones I and IV

[21] Inside the vegetated region (zone I), the flow is laterally uniform and the spatially and temporally averaged velocity, U_1 is determined from (5a), which simplifies to a balance between the drag and the surface or bed gradient, S,

$$U_1 = \sqrt{\frac{2gS}{C_D a}}. \tag{6}$$

[22] In the main channel, outside the region of shear (zone IV), the flow is uniform and given by a balance between the bed resistance and the gradient,

$$U_2 = \sqrt{\frac{2gSh}{c_f}}. \tag{7}$$

4.2. Inner Layer: Zone II

[23] Across the interface, there is very high shear as the flow rapidly transitions from the fast channel flow to the slow obstructed flow within the vegetation. The velocity profile within this narrow inner layer exhibits the inflection point and structure characteristic of a mixing layer, and is well-described by the hyperbolic tangent shear profile,

$$U_I = U_1 + U_s\left(1 + \tanh\left(\frac{y - y_o}{\delta_I}\right)\right), \tag{8}$$

where y_o is the inflection point, U_s is the slip velocity, $U_s = U(y_o) - U_1$, and δ_I is the inner layer width. This profile, shown in Figure 5a to closely match the the measured inner layer profiles, is well-established for describing canopy flows (see discussion in section 3.2). We estimate δ_I, y_o and U_s for each velocity profile by a nonlinear regression to (8) (MATLAB NLINFIT.M). Within the experimental resolution, $y_o \approx 0$ except for the sparsest array ($\phi = 0.02$), for which $y_o \approx 2d$ (see Table 1). In natural settings, this offset will always be much smaller than the length scale of the main channel, thus we can take $y_o = 0$ for modeling purposes.

[24] In *White and Nepf* [2007] the inner layer width, δ_I was shown to be independent of the main channel characteristics, but strongly correlated to the vegetation drag, $C_D a$, which can be inverted to form a length scale, $(C_D a)^{-1}$. A balance of drag and shear stress across the vegetation interface in (5a) suggests that this length scale establishes the penetration width, $\delta_I \sim (C_D a)^{-1}$ (this scaling has also been demonstrated for canopies by *Nepf et al.* [2007] and *Poggi et al.* [2004]). This dependence can be seen for sparse vegetation ($C_D ad \lessapprox 1$) in Figure 10, which also shows the

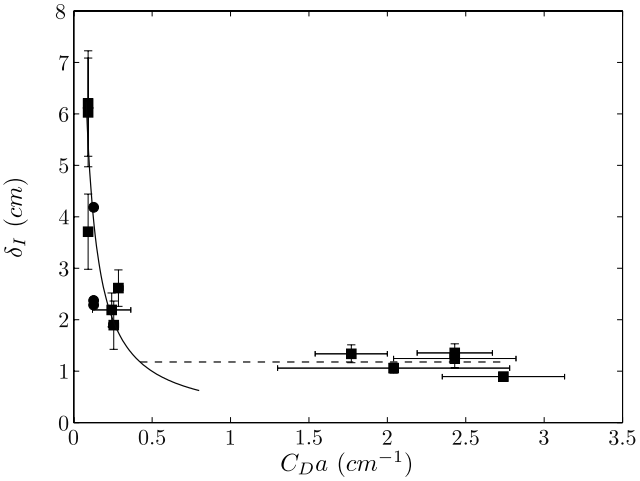

Figure 10. Inner layer width, δ_I, versus drag parameter, $C_D a$, present experiments (solid squares) and experiments of *Tsujimoto et al.* [1995] (solid circles). The best fit lines in the sparse vegetation limit, $\delta_I = 0.5(C_D a)^{-1}$ (solid line), and in the dense vegetation limit, $\delta_I = 1.8d$ (dashed line) are also shown. Error bars for the present experiments reflect uncertainty in measurements of both C_D and δ_I.

best fit line, $\delta_I = 0.5(C_D a)^{-1}$. Data from the similar experiments of *Tsujimoto et al.* [1995] are included in the plot (but not used in the fit) and agree well. For large values of $C_D a$, specifically when $(C_D a)^{-1}$ becomes less than the cylinder diameter, d, the penetration length scale, δ_I, becomes independent of $C_D a$. Physically, the velocity transition cannot occur over a distance less than that first row of cylinders, and thus the cylinder diameter places a lower limit on δ_I. The data suggest that $\delta_I \approx 1.8d$ in this high density region. Thus an empirical expression for the inner layer thickness is the maximum of the drag length scale and the cylinder diameter constraint,

$$\delta_I \approx \max\left(0.5(C_D a)^{-1}, 1.8d\right). \tag{9}$$

4.3. Outer Layer: Zone III

[25] As discussed in section 3.2, the outer (boundary) layer is independent of the inner layer. In the outer region the lateral shear stress approximately balances the pressure gradient from the free surface slope. A scaling relationship for the outer layer width, δ_O, is thus established by setting the pressure gradient and shear stress gradient from the momentum balance (5a) to be of the same order,

$$\frac{\partial\langle\overline{u'v'}\rangle}{\partial y} \sim gS, \tag{10}$$

and from (7), $gS = c_f U_2^2/(2h)$. Then using (3) to scale the shear stress gradient as u_*^2/δ_O, we arrive at the expression

$$\delta_O \sim \frac{u_*^2}{U_2^2}\frac{2h}{c_f}. \tag{11}$$

This scaling was confirmed in *White and Nepf* [2007].

[26] An expression for the velocity profile in the outer layer can also be determined from the momentum balance (5a). A model for the turbulent Reynolds stress is needed, and we show in section 6.3 that a constant eddy viscosity model is appropriate. Thus, in the outer layer, (5) can be rewritten as

$$-gS = \nu_t \frac{d^2 U_O}{dy^2} - \frac{c_f}{2h} U_O^2 \tag{12}$$

where the outer region velocity is denoted U_O, and is subject to the boundary conditions

$$U_O(y) \to U_2,\ y \to \infty \tag{13a}$$

and

$$U_O(y_m) = U_m \tag{13b}$$

[27] The virtual origin, y_m is defined as the point at which the outer layer velocity and its slope matches the inner layer velocity and its slope, to be determined below. The differential equation (12) has a solution given by

$$\frac{U_O}{U_2} = 3\tanh^2\left[\sqrt{\frac{3}{4(U_m/U_2+2)}}(y-y_m)/\delta_O + C\right] - 2 \tag{14}$$

where

$$C = \tanh^{-1}\sqrt{1+\frac{U_m/U_2-1}{3}} \tag{15}$$

and

$$\delta_O = \sqrt{\frac{3}{2(U_m/U_2+2)}}\frac{2h}{c_f}\frac{\nu_t}{U_2} \tag{16}$$

is the outer layer width, which we define from the slope at the matching point (see Figure 6) as,

$$\delta_O = \frac{U_2 - U_m}{\left.\frac{d\langle\overline{U}\rangle}{dy}\right|_{y_m}}. \tag{17}$$

[28] In section 7, after developing a model for the eddy viscosity, ν_t, it is shown that the expression (16) for the outer layer width is consistent with the scaling relation (11). The matching point, y_m is the point at which the slope of the inner and outer layers match. From (8), the inner layer slope is

$$\left.\frac{dU_I}{dy}\right|_{y_m} = \frac{U_s}{\delta_I}\left(1-\tanh^2\left(\frac{y_m - y_o}{\delta_I}\right)\right) \tag{18}$$

and from (17), the corresponding outer layer slope is $(U_2 - U_m)/\delta_O$. Setting them equal yields

$$U_m = U_2 - U_s\frac{\delta_O}{\delta_I}\left(1-\tanh^2\left(\frac{y_m - y_o}{\delta_I}\right)\right) \tag{19}$$

and from the inner layer profile,

$$y_m = \delta_I\left[\tanh^{-1}\left(\frac{U_m - U_1}{U_s} - 1\right)\right] + y_o. \tag{20}$$

[29] Based on the experimental results described in section (3.2) $y_o \approx 0$ and y_m is determined from (20) once U_m is known. Thus the two desired quantities are the matching velocity, U_m and the boundary layer width, δ_O and there are two equations: (16) and (19). However these equations also contain two additional unknowns: the slip velocity, U_s, and the eddy viscosiy, ν_t. The slip velocity is a property of the inner layer, and cannot be determined *a priori*, but a semiempirical expression is derived in the following section. The eddy viscosity is established by the turbulence driven by the shear layer vortices, and a model for it is developed in section 6.3.

5. Slip Velocity

[30] The slip velocity is determined in a semiempirical manner by matching the experimental velocity profiles in the inner and outer layers. First, the outer layer width, δ_O, and the matching point, y_m, are determined iteratively by

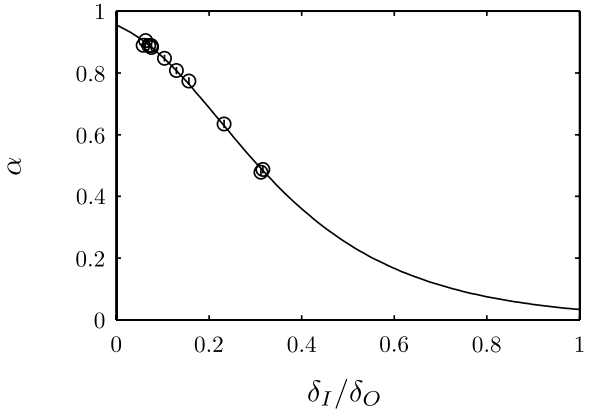

Figure 11. Normalized matching point, α, versus δ_I/δ_O for all experiments along with the best fit, $\tanh[c_1 \exp(-c_2\frac{\delta_I}{\delta_O})]$, where $c_1 = 1.89 \pm 0.03$, $c_2 = 4.03 \pm 0.08$.

fitting the experimental outer velocity profiles to the quadratic boundary profile shown in Figure 5,

$$U_O = U_m + (U_2 - U_m)\left[\frac{y - y_m}{\delta_O} - \frac{1}{4}\left(\frac{y - y_m}{\delta_O}\right)^2\right], \qquad (21)$$

where y_m is the point at which the inner and outer slopes match, $dU_I/dy = dU_O/dy$, and $U_m = U_O(y_m)$. Because this profile fits the measured outer layer profiles so well (see Figure 5b) and because it is mathematically simple, it is used here for matching with the inner layer profiles in order to determine y_m, δ_O, and U_s. From the experimental data, we determine δ_O and y_m iteratively by (1) guessing y_m, (2) performing a quadratic regression in the outer region to determine δ_O, and (3) repeating with a new y_m until the inner and outer layer slopes match at y_m. The width, δ_O is determined from the slope at the matching point according to (17). Figure 6 demonstrates the matching between the inner and outer layers for a representative velocity distribution.

[31] The experimental results for the matching point, y_m, are shown in Figure 11, expressed in terms of the parameter α,

$$\alpha = \tanh\left(\frac{y_m - y_o}{\delta_I}\right), \qquad (22)$$

which is chosen because of the hyperbolic tangent form of the inner layer velocity profile (8). The best fit to the data is of the form

$$\alpha = \tanh[1.89\exp(-4.03\delta_I/\delta_O)]. \qquad (23)$$

[32] In the limit $\delta_I/\delta_O \to 0$ (dense vegetation), the velocity gradient in the boundary layer is much less than in the inner layer, so $\alpha \to 1$, i.e., the point where the slopes match is on the flat part of the tanh inner layer profile. However, for $\delta_I/\delta_O \to 1$ (sparse vegetation), the outer and inner layer are comparable and $\alpha \to 0$, i.e. the matching point is near the inflection point, y_o, of the tanh profile.

[33] Given y_m, the slip velocity, U_s, is obtained by matching the inner layer hyperbolic tangent profile (8) and the outer layer quadratic profile (21) at y_m, to yield

$$U_s = \frac{\delta_I}{\delta_O}\frac{U_2 - U_1}{(1 - \alpha^2) + (1 + \alpha)\frac{\delta_I}{\delta_O}}. \qquad (24)$$

[34] The resulting semiempirical prediction for U_s is shown along with the experimental measurements in Figure 12. Although the expression (24) relies on data to determine α, it's behavior is nonetheless illuminating. Across the range of array densities in the present experiments, $U_s/(U_2 - U_1)$ increases weakly with δ_I/δ_O. The data from the submerged canopy experiments of *Ghisalberti and Nepf* [2004] are also shown for comparison, and are also close to the prediction. Outside the limits of the data, the behavior of U_s is intuitive, approaching zero as $\delta_I/\delta_O \to 0$, which is the limit of vegetation so dense it resembles a solid (no-slip) wall; and slowly approaching $U_s/(U_2 - U_1) = 0.5$ in the sparse array limit ($\delta_I/\delta_O \to 1$), which is the limit of a symmetric mixing layer.

6. Shear Stress Distribution

6.1. Vortex-Induced Exchange

[35] In order to close the momentum balance, it is necessary to predict the shear stress distribution. Of particular importance is u_*, the lateral friction velocity, which describes the momentum exchange at the interface. As discussed in section 3.3, the vortices are the dominant contributors to this momentum exchange. Referring to Figure 8, the vortices primarily occupy the main channel (zone III), with a width that scales with δ_O, and exchange fluid between the vegetation and the main channel through the exchange zone (zone II). Because the vortices are periodic, the lateral flux of mass or momentum is proportional to the fluid volume, V_e, exchanged in one wavelength, L, over one period, $T_d = 1/f_d$. As a vortex passes a reach of length L, it induces an ejection from the vegetation which

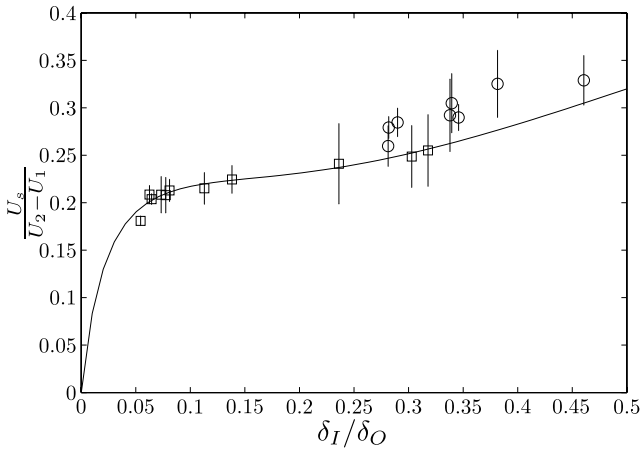

Figure 12. Normalized slip velocity, $U_s/(U_2 - U_1)$ plotted with the semiempirical expression (24). Results from all experimental velocity profiles in the present experiments shown in squares; results from *Ghisalberti and Nepf* [2004] shown in circles.

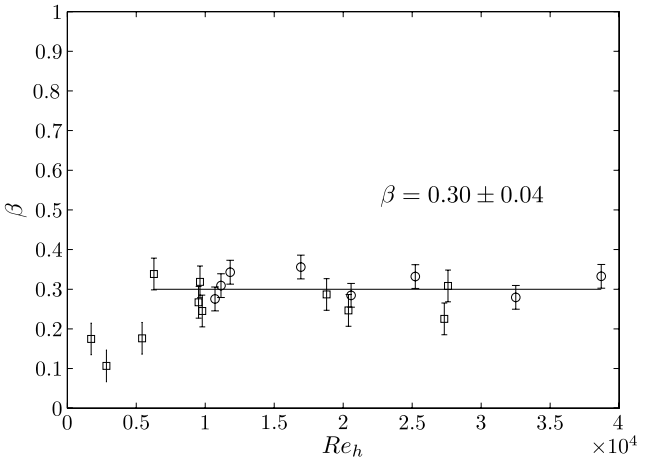

Figure 13. Values of the the vortex exchange ratio, β plotted with depth Reynolds number, $Re_h = \Delta U h/\nu$. Values are obtained from the submerged canopy tracer experiments of *Ghisalberti and Nepf* [2005] (open circles) and from u_*^2 in the present experiments (open squares).

entrains the fluid volume V_e (see Figure 9). Mass conservation requires an equal volume of fluid be transported from the free stream into the vegetation by a sweep. The entrained volume, V_e, must scale with the vortex volume itself, hence

$$V_e = \beta \delta_O L h, \tag{25}$$

where β is the factor of proportionality that describes the efficiency of exchange. Physically, β represents the fraction of the vortex volume that is lost and replaced as it travels a distance equal to its wavelength, L. Dividing by the interfacial area along the channel reach, hL, and the period of each vortex cycle, T_d yields the average rate of volumetric flux of fluid per unit interfacial area,

$$k = \frac{V_e}{hLT_d} = \frac{\beta \delta_O}{T_d}. \tag{26}$$

[36] The units of k are of velocity, representing a mass transfer, or exchange, coefficient. Using the vortex frequency (4), the exchange coefficient can be written

$$k = \beta \delta_O \frac{0.032\overline{U}}{\theta}. \tag{27}$$

[37] The exchange ratio, β was determined both from measurements of momentum exchange in the present experiments and also from measurements of mass exchange in the dye studies by *Ghisalberti and Nepf* [2005] in a submerged vegetated canopy (see reference for details of the scalar experiments). They used a two-layer model to evaluate the mass flux, J_s, between the vegetation (layer 1) and the overlying fluid (layer 2),

$$J_s = -k\Delta C = -\beta \frac{\delta_O}{T_d} \Delta C \tag{28}$$

where $\Delta C = C_2 - C_1$ is the concentration difference between the two layers. By analogy, the momentum exchanged by the vortices is proportional to the velocity difference between the layers, ΔU, and thus the flux is

$$J_s = -\gamma k \Delta U = -\gamma \beta \frac{\delta_O}{T_d} \Delta U \tag{29}$$

γ is the ratio of the momentum to mass flux, typically less than one due to influence of pressure fluctuations on momentum, but not scalar, transport [see *Hinze*, 1975]. By comparing the mass flux to the momentum flux in the submerged canopy experiments of *Ghisalberti and Nepf*, the parameter γ was determined to be $\gamma = 0.8 \pm 0.1$. The momentum flux at the vegetation interface is by definition equal to the turbulent Reynolds stress (viscous stresses are negligible by comparison and there is no direct lateral advective flux in the mean since $\langle \overline{U} \rangle$ is unidirectional),

$$J_s = \langle \overline{u'v'} \rangle \big|_{y=0} = -u_*^2. \tag{30}$$

which yields an expression for the lateral friction velocity

$$u_*^2 = \gamma \beta \frac{\delta_O}{T_d} \Delta U. \tag{31}$$

[38] The estimates of the exchange ratio, β from both the present experiments and the submerged canopy experiments of *Ghisalberti and Nepf* are shown in Figure 13 as a function of Reynolds number. The value of β is approximately constant above $Re_h \approx 0.5 \times 10^4$. For the three cases with $Re_h < 0.5 \times 10^4$, β is lower by at least a factor of two, likely due to the weakening of vortices by bottom friction, which is more pronounced at low Reynolds number due to viscous effects. The high Reynolds cases are closer to natural channels, with flow depths on the order of meters and velocities on the order of 1 m/s yielding Reynolds numbers of at least 10^6. Thus, only the high Re_h data for both the shallow and submerged experiments have been averaged to obtain a mean exchange ratio of $\beta = 0.30 \pm 0.04$.

[39] The constant value of β across all high Reynolds number experiments suggests that vortices at the edge of shallow vegetation are similar to vortices at the top of a submerged canopy in their ability to transport mass and momentum, independent of vegetation density, and that exchange is described quite well by (27). This is reinforced in the following section by field and experimental results for the lateral friction velocity across a range of vegetation canopies.

6.2. Interfacial Shear Stress

[40] The results for β can be combined with the exchange coefficient, k, to predict the shear stress at the vegetation interface. From (31) and the expression for the vortex passage frequency (4), the shear stress at the interface is

$$-\tau_i/\rho = u_*^2 = 0.032\beta\gamma \frac{\delta_O}{\theta} \overline{U} \Delta U. \tag{32}$$

[41] A lateral friction coefficient for the vegetation-main channel interface can be defined as,

$$f_i = \frac{u_*^2}{\frac{1}{2}(\Delta U)^2} = 0.032\beta\gamma \frac{\delta_O}{\theta} \frac{1}{R}, \tag{33}$$

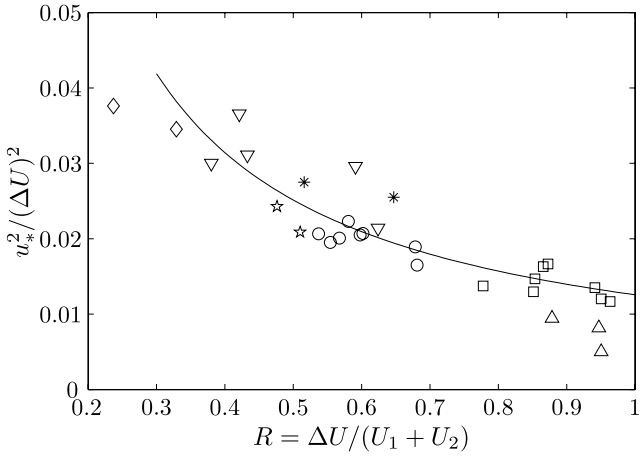

Figure 14. Interfacial shear stress, $u_*{}^2/(\Delta U)^2 = f_i/2$ plotted versus the dimensionless velocity ratio, $R = \Delta U/(U_1 + U_2)$. Experimental data collected from the present experiments (open squares, open upward pointing triangles–low Re_θ), the shallow vegetated channel experiments of *Tsujimoto et al.* [1995], and submerged canopies: *Ghisalberti and Nepf* [2005] (open circles), *Dunn et al.* [1996]: rigid cylinders (open downward pointing triangles), flexible strips (stars), *Nepf and Vivoni* [2000] (asterisks). The solid line is the semiempirical prediction from (33).

where R is the velocity difference, $R = (U_2 - U_1)/(U_2 + U_1)$. The friction coefficient is thus inversely proportional to the velocity difference, R. We have compiled data for u_* from experiments in shallow vegetated channels and from the literature on submerged canopies in flumes and wind tunnels, and the results are plotted in Figure 14. The curve represents the semiempirical prediction (33) using the parameters $\beta = 0.3$, $\gamma = 0.8$, and δ_O/θ taken as the average value across all of the velocity distributions from the present experiments and those from *Ghisalberti and Nepf* [2005], ($\delta_O/\theta \approx 3.3 \pm 0.4$). The prediction from (33) describes the data remarkably well, capturing the decline in friction coefficient with increasing velocity ratio. Presumably due to the increased resistance acting against the vortices, denser canopies, with higher R, result in lower momentum transport (smaller f_i). It is concluded that the expression (33) should be broadly applicable in describing the shear stress at the edge of shallow emergent vegetation. Moreover, it supports the use of the parameters $\delta_O \approx 3.3$, $\beta \approx 0.3$ and $\gamma \approx 0.8$ for a range of vegetation conditions. On this basis, we will use these parameter values to model the velocity and shear stress distributions in section 7.

6.3. Shear Stress Closure

[42] In order to close the momentum balance, a parameterization for the shear stress distribution in the main channel is needed. Eddy viscosity or mixing length formulations are most commonly used for this purpose. For all LDV transects we have calculated the lateral distribution of eddy viscosity,

$$\nu_t = -\langle \overline{u'v'} \rangle \Big/ \frac{\partial \langle \overline{U} \rangle}{\partial y}, \tag{34}$$

and mixing length,

$$L_m = -\langle \overline{u'v'} \rangle \Big/ \left(\frac{\partial \langle \overline{U} \rangle}{\partial y} \right)^2. \tag{35}$$

[43] First, $\overline{u'v'}$ and $\overline{U}(y)$ were smoothed with a moving-average filter. Estimates of $\partial\langle\overline{U}\rangle/\partial y$ were then obtained by the central difference method. Each is normalized using the outer layer length scale, δ_O, the outer layer velocity scale, $U_2 - U_m$, and the lateral friction velocity, u_*,

$$\nu_t^* = \frac{\nu_t (U_2 - U_m)}{\delta_O u_*^2} \tag{36a}$$

and

$$L_m^* = \frac{L_m (U_2 - U_m)}{\delta_O u_*}, \tag{36b}$$

and are plotted versus the normalized outer layer coordinate in Figures 15a and 15b. Both ν_t^* and L_m^* are $O(1)$ in the central region of the shear layer, suggesting that the scaling is appropriate. Due to division by small values of $d\langle\overline{U}\rangle/dy$, the estimates for ν_t and L_m become erratic outside the shear layer, and thus we plot values only up to $(y - y_o)/\delta_O = 1.3$.

[44] The eddy viscosity (15a) peaks just outside the interface at $y/\delta_O \approx 0.2$, where the coherent structures are strongest. Moving into the vegetation, ν_t declines sharply, with very small values for $y < 0$, as momentum is unable to substantially penetrate the obstructions. In the main channel, ν_t is much larger and decreases slightly away from the peak.

[45] The mixing length (15b) also declines sharply moving into the vegetation, suggesting that the turbulent length scale sharply transitions from that of the coherent shear layer structures in the main channel, to that of stem wakes in the vegetation. In the open channel the mixing length for each experimental case is approximately constant.

[46] The data suggests that either a constant mixing length model or constant eddy viscosity may be used to reasonably model the flow in the channel. The mean mixing length across all cases within the outer layer, $(y - y_o)/\delta_O > 0$, is $L_m^* = 0.75 \pm 0.13$ and the mean eddy viscosity is $\nu_t^* = 0.7 \pm 0.15$. The theory for the outer layer velocity presented in section 4.3 utilizes a constant eddy viscosity closure for the shear stress, and based on the experimental results described here, the form

$$\nu_t = \frac{0.7 u_*^2 \delta_O}{U_2 - U_m}, \tag{37}$$

will lead to the best prediction of the outer layer velocity profile.

7. Mean Velocity Prediction

[47] Having obtained expressions for the inner layer width, δ_I, the interfacial slip velocity, U_s, the interfacial shear stress, u_*^2, and a closure for the shear stress distribution, the mean velocity distribution across a partially vegetated channel can be predicted.

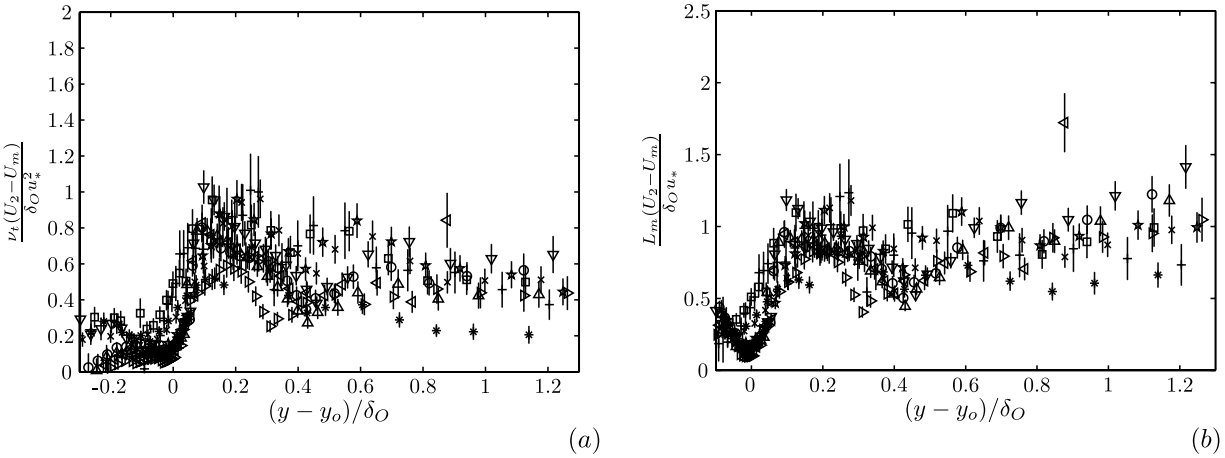

Figure 15. Profiles of normalized eddy viscosity (a) and mixing length (b), for all experimental profiles plotted in outer layer coordinates. The uncertainty, shown in bars, is due primarily to division by the local velocity gradient, prone to strong fluctuations. Specific symbols correspond to these runs: open squares (case I), pluses (case III), crosses (case IV), asterisks (case V), stars (case VI), open circles (case VII), open upward pointing triangles (case VIII), open downward pointing triangles (case IX), open left pointing triangles (case X), and open right pointing triangles (case XI).

[48] The free stream velocity, U_2, can be calculated from the bed drag-surface slope balance in the uniform flow region outside the shear layer (7) and the velocity within the vegetation, U_1, is similarly determined from (6). These expressions require estimates of the channel friction coefficient, c_f and the plant stem density, a, and drag coefficient, C_D. The friction coefficient is a common measure for open channels and is typically about 1×10^{-3}, but for simplicity in modeling field conditions, a good estimate can be made from a well-placed measurement of the velocity at the channel center and the channel bottom slope using (7). Measurements of resistance due to emergent vegetation in open channels are increasingly available [*Lee et al.*, 2004; *Struve et al.*, 1996]. However, since $C_D \approx 1$ in most cases, it is often possible to use a alone in the vegetation drag expression (6) if measures of the plant biomass density alone are available [*Lightbody and Nepf*, 2006]. Moreover, in the field a simple estimate of $C_D a$ and δ_I could be obtained directly by measuring the penetration of velocity or flow structures from the main channel into the vegetation (δ_I) using the relation $\delta_I \approx 0.5(C_D a)^{-1}$ [see *Nepf et al.*, 2007]. The assumption of fully developed flow also permits use of the expression

$$\frac{c_f}{h} = C_D a \frac{U_1^2}{U_2^2}, \tag{38}$$

which provides a method of calculating c_f if the vegetation properties and estimates of the mid-channel and within-vegetation velocity are known, or conversely of calculating the vegetation drag, $C_D a$ if the channel drag and velocities are known.

[49] Given the vegetation drag properties, from section 4.2 the inner layer width, δ_I can be calculated by

$$\delta_I = \max\left(c_1(C_D a)^{-1},\ c_2 d\right) \tag{39}$$

where the empirical results $c_1 = 0.5$, $c_2 = 1.8$ were obtained from the present experiments.

[50] Next, the outer layer width, δ_O and the matching velocity, U_m are determined by solving (17) and (19) along with the expression for the slip velocity, (24). Using the eddy viscosity expression (37) an explicit equation results for δ_O,

$$\delta_O = \frac{3 \times 0.7}{2(U_m/U_2 + 2)(1 - U_m/U_2)} \frac{2h}{c_f} \frac{u_*^2}{U_2^2} \tag{40}$$

[51] Notice first that the behavior of δ_O is exactly that predicted by the simple scaling argument (11), with an $O(1)$ factor that depends weakly on U_m/U_2 multiplying the original scaling prediction $\delta_O \sim (2h/c_f)(u_*^2/U_2^2)$. The interfacial friction velocity, u_* is given by (3) as

$$u_*^2 = 0.032\beta\gamma \frac{\delta_O}{\theta} \frac{(U_1 + U_2)}{2} \Delta U. \tag{41}$$

with $\beta = 0.3$, $\gamma = 0.8$, and $\delta_O/\theta = 3.29$, as determined in section 6. Note that the expression $\delta_O/\theta = 3.29$ is essentially a shape factor, as it relates two length scales from the same velocity profile. This ratio is expected to be broadly applicable to vegetation layers, which possess very similar velocity profile shapes, and its success in predicting u_* for a range of vegetation types (see Figure 14) bears this out.

[52] The matching velocity is determined from (19), along with the expression for the slip velocity (24),

$$U_m = U_2 - \frac{U_2 - U_1}{1 + \frac{\delta_I/\delta_O}{(1-\alpha)}} \tag{42}$$

where the nondimensional matching point, α is given by (23),

$$\alpha = \tanh[1.89 \exp(-4.03\delta_I/\delta_O)]. \tag{43}$$

[53] The two equations for δ_O (40) and U_m (42) can be solved quite simply using Newton's method by substituting

the expression for δ_O (40) into (42) and using the expression (41) for u_* and (43) for α.

[54] Once U_m is obtained, y_m can be calculated from the inner layer profile by

$$y_m = \delta_I \left[\tanh^{-1} \left(\frac{U_m - U_1}{U_s} - 1 \right) \right] + y_o, \tag{44}$$

recalling that

$$U_s = \frac{\delta_I}{\delta_O} \frac{U_2 - U_1}{(1-\alpha^2) + (1+\alpha)\frac{\delta_I}{\delta_O}}. \tag{45}$$

[55] The velocity profile in the outer region is finally given by (14),

$$\frac{U_O}{U_2} = 3 \tanh^2 \left[\sqrt{\frac{3}{4(U_m/U_2 + 2)}} (y - y_m)/\delta_O + C \right] - 2 \tag{46}$$

where

$$C = \tanh^{-1} \sqrt{1 + \frac{U_m/U_2 - 1}{3}}. \tag{47}$$

[56] The profile in the inner region is given by (8)

$$U_I = U_1 + U_s \left(1 + \tanh \left(\frac{y - y_o}{\delta_I} \right) \right), \tag{48}$$

where y_o, the inflection point, is taken as the vegetated layer edge, consistent with experimental results. The inner and outer layer distributions can then be combined and meet at y_m, yielding the overall velocity profile.

[57] The Reynolds stress profile can also be calculated from the mean velocity profile. In the outer layer, from section 6.3 and by differentiating the velocity profile (46)

$$\langle \overline{u'v'} \rangle_O = \nu_t \frac{dU_O}{dy} = 0.7 u_*^2 \frac{U_2 - U}{U_2 - U_m} \sqrt{\frac{U + U_2}{U_m + U_2}}. \tag{49}$$

[58] In the inner layer, the eddy viscosity is reduced significantly as the drag from the vegetation reduces momentum transfer within the vegetation (see Figure 15). A simple model for ν_t in the inner layer is,

$$\nu_t = \frac{u_*^2 \delta_I}{U_s} \tag{50}$$

and thus δ_I is the length scale for momentum transfer. The Reynolds stress in the inner layer can thus be written

$$\langle \overline{u'v'} \rangle_I = \nu_t \frac{dU_I}{dy} = \frac{u_*^2 \delta_I}{U_s} \frac{dU_I}{dy} \tag{51}$$

which ensures that, by definition the interfacial shear stress is $\tau_i = u_*^2$. Because the eddy viscosity is different within the inner and outer layers, it is not possible to match the Reynolds stress at y_m, and there a stress transition region the modeling of which is beyond the scope of this paper. Nonetheless, the following demonstrates the inner and outer layer predictions for the stress distribution reproduce the experimental data well.

[59] The velocity and shear stress profiles were predicted using the preceding methodology and using only U_1, U_2, and $C_D a$ as inputs. Comparisons between the predicted and measured profiles are shown in Figure 16 for several cases. The comparison is quite good, confirming the validity of the model. Specifically, the total discharge provides a simple metric for comparison is the total discharge,

$$Q = \int_{y_1}^{y_2} U(y) dy, \tag{52}$$

where y_1 and y_2 are the limits of the measured velocity profile. The predicted discharge for each case is within 3% of the measured discharge for each of the profiles. Most importantly, the two-layer structure of the velocity profile is resolved. The model successfully captures the high shear in the inner region near the vegetation interface, and the transition to boundary layer flow in the main channel.

[60] The shear stress distributions are also predicted quite well, with the inner layer model capturing the sharp decline in Reynolds stress into the vegetation, and the sharp peak at the interface. The outer layer model captures the broad, slow decay in the main channel. As mentioned, there is a stress jump where the inner and outer regions meet, but the transition occurs over a very short distance, and it is clear that the outer and inner distributions can be patched together quite well to reproduce the observed Reynolds stress.

[61] An important assumption of the model is that the channel width exceeds the calculated width of the boundary layer. When met, this condition assures a constant velocity in the main channel outside the shear layer. All of our experimental cases in the 120-cm-wide flume meet this criterion. However, in a channel narrower than δ_O, there is no uniform velocity (U_2) region and the shear stress will enter into the momentum balance over the entire channel. In such cases the boundary condition (13b) must be changed to a no slip condition on the far wall. Nonetheless, the eddy viscosity model is often valid for closed conduits and should remain appropriate in this case as well, although the far wall can be expected to modify to some degree the coherent vortices and the turbulence structure.

8. Conclusions

[62] This paper presents an improved method for interpreting and predicting the velocity and shear stress in a channel adjacent to a vegetated floodplain. Such predictions are useful for studies of floodplain erosion and deposition, material transport, and channel conveyance. Expressions have been obtained for the profiles of velocity and turbulent shear stress across the entire channel and vegetation zone. Experimental measurements show the dominant feature of the flow is a two layer structure, with high shear across the vegetation interface and a more gradual boundary layer outside the vegetation. In addition, experiments demonstrate the strong influence of coherent vortex structures in exchanging momentum between the channel and vegetation. Using the vortex characteristics to predict momentum exchange, the model successfully captures the two layer

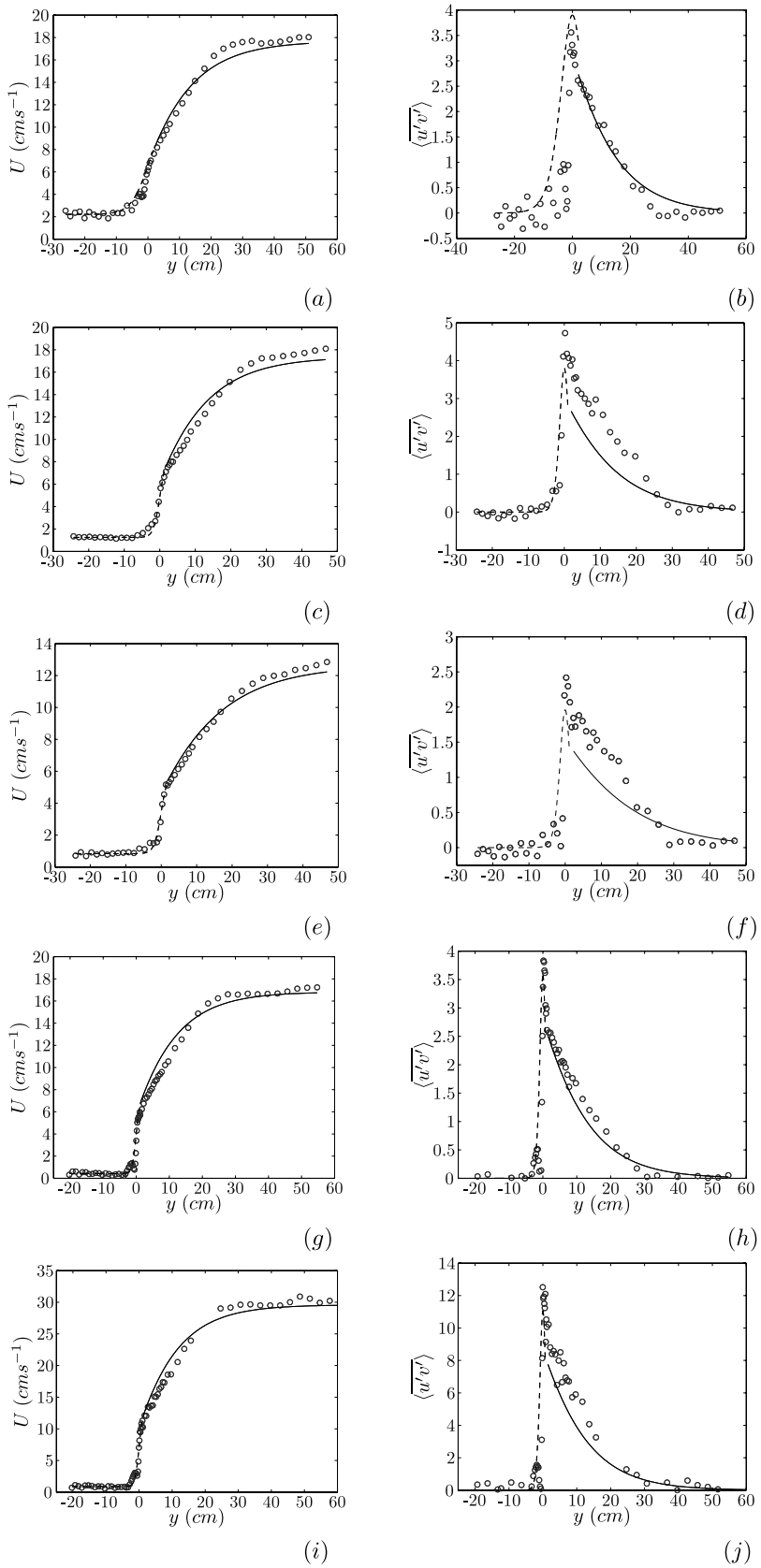

Figure 16. Experimental and predicted velocity and Reynolds stress distributions for cases I (a–b), IV (c–d), VI (e–f), VII (g–h) and X (i–j). Outer layer profiles (solid line) and inner layer profiles (dashed line) are distinguished. The predictions are made using the model described in section 7, using only U_1, U_2, and $C_D a$ as input.

structure. Previous studies have used models based on a constant eddy viscosity or one-dimensional integral methods which are not capable of resolving the two-layer structure adequately. Moreover, by focusing on the dynamics of the coherent structures, we are able to accurately predict the shear stress at the vegetation interface. This measure is not only essential in predicting the velocity distribution, but it also is important for studies of sediment transport, providing an estimate of the mass flux across the interface and the lateral stress on the vegetated bank. The vortices, and the turbulent fluxes they induce at the interface can be expected to play a dominant role in the transport of sediment onto the vegetated plain.

[63] **Acknowledgments.** This material is based upon work supported by the National Science Foundation under grant 0125056. Any opinions, findings, and conclusions or recommendations expressed in this material are those of the authors and do not necessarily reflect the views of the National Science Foundation.

References

Dunn, C., F. Lopez, and M. Garcia (1996), Mean flow and turbulence in a laboratory channel with simulated vegetation, technical report, Dep. of Civ. Eng., Univ. of Ill. at Urbana-Champaign.

Ghisalberti, M., and H. Nepf (2002), Mixing layers and coherent structures in vegetated aquatic flows, *J. Geophys. Res.*, *107*(C2), 3011, doi:10.1029/2001JC000871.

Ghisalberti, M., and H. Nepf (2004), The limited growth of vegetated shear layers, *Water Resour. Res.*, *40*, W07502, doi:10.1029/2003WR002776.

Ghisalberti, M., and H. Nepf (2005), Mass transport in vegetated shear flows, *Environ. Fluid Mech.*, *5*(6), 527–551.

Helmiö, T. (2004), Flow resistance due to lateral momentum transfer in partially vegetated rivers, *Water Resour. Res.*, *40*, W05206, doi:10.1029/2004WR003058.

Hinze, J. O. (1975), *Turbulence*, 2nd ed., McGraw-Hill, New York.

Ho, C.-M., and P. Huerre (1984), Perturbed free shear layers, *Ann. Rev. Fluid Mech.*, *16*, 365–424.

Ikeda, S., N. Izumi, and R. Ito (1991), Effects of pile dikes on flow retardation and sediment transport, *J. Hydraul. Eng.*, *117*(11), 1459–1478.

Katul, G., P. Wiberg, J. Albertson, and G. Hornberger (2002), A mixing layer theory for flow resistance in shallow streams, *Water Resour. Res.*, *38*(11), 1250, doi:10.1029/2001WR000817.

Lee, J. K., L. C. Roig, H. L. Jenter, and H. M. Visser (2004), Drag coefficients for modeling flow through emergent vegetation in the Florida Everglades, *Ecol. Eng.*, *22*(4–5), 237–248.

Lightbody, A. F., and H. M. Nepf (2006), Prediction of velocity profiles and longitudinal dispersion in emergent salt marsh vegetation, *Limnol. Oceanogr.*, *51*(1).

Nadaoka, K., and H. Yagi (1998), Shallow-water turbulence modeling and horizontal large-eddy computation of river flow, *J. Hydraul. Eng.*, *124*(5), 493–500.

Nepf, H. M., and E. R. Vivoni (2000), Flow structure in depth-limited, vegetated flow, *J. Geophys. Res.*, *105*(C12), 28,527–28,546.

Nepf, H., M. Ghisalberti, B. White, and E. Murphy (2007), Retention time and dispersion associated with submerged aquatic canopies, *Water Resour. Res.*, *43*, W04422, doi:10.1029/2006WR005362.

Nezu, I., and K. Onitsuka (2000), Turbulent structures in partly vegetated open-channel flows with lda and piv measurements, *J. Hydraul. Res.*, *39*(6), 629–642.

Nikora, V., K. Koll, I. McEwan, S. McLean, and A. Dittrich (2002), Velocity distribution in the roughness layer of rough-bed flows, *J. Hydraul. Eng.*, *130*(10), 1036–1042.

Pasche, E., and G. Rouvé (1985), Overbank flow with vegetatively roughened floodplains, *J. Hydraul. Eng.*, *111*(9), 1262–1278.

Poggi, D., A. Porporato, and L. Ridolfi (2004), The effect of vegetation density on canopy sub-layer turbulence, *Boundary Layer Meteorol.*, *111*, 565–587.

Raupach, M., J. Finnigan, and Y. Brunet (1996), Coherent eddies and turbulence in vegetation canopies: The mixing layer analogy, *Boundary Layer Meteorol.*, *78*, 351–382.

Struve, J., R. A. Falconer, and Y. Wu (1996), Influence of model mangrove trees on the hydrodynamics in a flume, *Estuarine Coastal Shelf Sci.*, *58*(1), 163–171.

Tamai, N., T. Asaeda, and H. Ikeda (1986), Study on generation of periodical large surface eddies in a composite channel flow, *Water Resour. Res.*, *22*(7), 1129–1138.

Tsujimoto, T., A. Tsuji, N. Izumi, and T. Okada (1995), KHL progressive report: Characteristics of flow in the transitional reach of a stream with a vegetation zone along a side wall, technical report, Kanazawa Univ., Kanazawa, Japan.

van Prooijen, B., J. Battjes, and W. Uijttewaal (2005), Momentum exchange in straight uniform compound channel flow, *J. Hydraul. Eng.*, *131*(3), 177–185.

Vionnet, C., P. Tassi, and J. M. Vide (2004), Estimates of flow resistance and eddy viscosity coefficients for 2d modelling on vegetated floodplains, *Hydrol. Processes*, *18*, 2907–2926.

White, B., and H. Nepf (2007), Shear instability and coherent structures in shallow flow adjacent to a porous layer, *J. Fluid Mech.*, in press.

Xiaohui, S., and C. Li (2002), Large eddy simulation of free surface turbulent flow in partly vegetated open channels, *Int. J. Numer. Methods Fluids*, *39*, 919–937.

H. M. Nepf, Department of Civil and Environmental Engineering, Massachusetts Institute of Technology, Cambridge, MA 02139, USA. (hmnepf@mit.edu)

B. L. White, Department of Physical Oceanography, Woods Hole Oceanographic Institution, Woods Hole, MA 02543, USA. (bwhite@whoi.edu)